

Discovery and Timing of Four γ -ray Millisecond Pulsars

M. KERR,¹ S. JOHNSTON,² C. J. CLARK,^{3,4} F. CAMILO,⁵ E. C. FERRARA,^{6,7,8} M. T. WOLFF,¹ S. M. RANSOM,⁹ S. DAI,²
P. S. RAY,¹ J. E. REYNOLDS,² J. M. SARKISSIAN,² E. D. BARR,¹⁰ M. K. KRAMER,^{10,11} AND B. W. STAPPERS¹¹

¹Space Science Division, Naval Research Laboratory, Washington, DC 20375–5352, USA

²Australia Telescope National Facility, CSIRO, Space and Astronomy, PO Box 76, Epping, NSW 1710, Australia

³Max Planck Institute for Gravitational Physics (Albert Einstein Institute), D-30167 Hannover, Germany

⁴Leibniz Universität Hannover, D-30167 Hannover, Germany

⁵South African Radio Astronomy Observatory (SARAO), 2 Fir Street, Observatory, Cape Town 7925, South Africa

⁶Department of Astronomy, University of Maryland, College Park, MD 20742, USA

⁷Center for Research and Exploration in Space Science and Technology, NASA/GSFC, Greenbelt, MD 20771, USA

⁸NASA Goddard Space Flight Center, Greenbelt, MD 20771, USA

⁹National Radio Astronomy Observatory, 520 Edgemont Road, Charlottesville, VA 22903-2475, USA

¹⁰Max-Planck-Institut für Radioastronomie, Auf dem Hügel 69, D-53121 Bonn, Germany

¹¹Jodrell Bank Centre for Astrophysics, Department of Physics and Astronomy, University of Manchester, Manchester M13 9PL, UK

ABSTRACT

We discovered four millisecond pulsars (MSPs) in searches of 80 γ -ray sources conducted from 2015 to 2017 with the *Murriyang* radio telescope of the Parkes Observatory. We provide an overview of the survey and focus on the results of a follow-up pulsar timing campaign. Using *Fermi* Large Area Telescope data, we have detected γ -ray pulsations from all four pulsars, and by combining radio and γ -ray data we obtain improved timing solutions. We also provide flux density distributions for the radio pulsars and flux-calibrated and phase-aligned radio and γ -ray pulse profiles. Some of the pulsars may be suitable for radio pulsar timing array experiments. PSR J0646–5455, PSR J1803–4719, and PSR J2045–6837 are in typical, nearly circular white dwarf binaries with residual eccentricities proportional to their binary periods. PSR J1833–3840 is a black widow pulsar with the longest known period, $P_b = 0.9$ d, and a very soft radio spectrum. PSR J0646–5455 has a strong, Vela-like γ -ray pulse profile and is suitable for inclusion in the γ -ray Pulsar Timing Array (GPTA). Despite this, it is possibly one of the lowest-efficiency γ -ray MSPs known. Indeed, all four new γ -ray MSPs have lower-than-average efficiency, a potential indication of bias in earlier searches. Finally, we retrospectively evaluate the efficiency of this survey: while only four new MSPs were directly discovered, subsequent campaigns have found pulsars in a further 19 of our targets, an excellent 30% efficiency.

1. INTRODUCTION

Since the launch of the *Fermi* Large Area Telescope (LAT, Atwood et al. 2009) in 2008, γ -ray pulsations have been detected from more than 300 pulsars (Smith et al. 2023). Nearly half of these are millisecond pulsars (MSPs). Unlike the most populous γ -ray source class, blazars, the emission from pulsars does not vary on long timescales, and it manifests a nearly universal spectral shape peaking around 1 GeV. It is thus possible to identify pulsar-like LAT sources and target them for deep and repeated radio pulsation searches (Ray et al. 2012), an approach which has led to the discovery of well over 100 MSPs.

Targeted observations enable longer integrations compared to wide-area pulsar surveys, yielding increased sensitivity to faint pulsars. Repeating the observations yields further advantages. All pulsars scintillate in the ionized interstellar medium (e.g. Narayan 1992) with concomitant variations in received flux at the earth. Observing during a scintillation minimum reduces the chances of discovering a pulsar, and vice versa. Furthermore, a growing subset of MSPs are found in compact binaries, in which ionized material lifted from the companion surface by the energetic pulsar wind can eclipse radio emission for substantial fractions of the orbit (e.g. Polzin et al. 2020). Because the γ rays are generally unaffected unless there is a direct eclipse (Clark et al. 2023), targeting pulsar-like LAT sources has proven to be a particularly effective way of finding these binaries (e.g. Bangale et al. 2024).

Once a pulsar is found in a search of a γ -ray source, a timing campaign with a radio telescope is generally

needed to establish the pulsar spin frequency ν , spin-down rate $\dot{\nu}$, position, and Keplerian parameters with sufficient precision to accurately predict the pulsar spin phase at any given time—i.e. to obtain a timing solution. A timing solution enables γ -ray folding—mapping of LAT photon time stamps to spin phase—which in turn allows a pulse profile to emerge from the noise.

Four MSPs were discovered nearly ten years ago in a Parkes campaign targeting LAT sources, but the follow-up was insufficient to produce good timing solutions. These are PSR J0646–5455, previously known as PSR J0646–54 in the ATNF pulsar catalog (psrcat, Manchester et al. 2005) and noted as a likely γ -ray pulsar in the third LAT pulsar catalog (3PC, Smith et al. 2023); PSR J1803–4719, not previously in psrcat and listed as PSR J1802–4719 in 3PC; PSR J1833–3840, listed as same in both psrcat and 3PC; and PSR J2045–6837, listed as same in 3PC but as PSR J2045–68 in psrcat.

Because of potential for bolstering the complement of MSPs available for the γ -ray Pulsar Timing Array (GPTA, Ajello et al. 2022), we were motivated to obtain new data from the *Murriyang* radio telescope at the Parkes Observatory. With it, archival data, and new techniques for phase connection, we have obtained good timing solutions and detected γ -ray pulsations from all four MSPs. The detection and pulse profile for J1833–3840 were already reported in 3PC, but we provide a characterization of its radio properties and a much-improved timing solution and γ -ray pulse profile.

Below, we present an overview of the unpublished details of the pulsar search campaigns which detected the MSPs (§2); describe the original and updated radio timing campaigns (§3); discuss the detection of γ -ray pulsations and improved timing thereby enabled; present multi-wavelength properties (§5); and discuss the resulting timing solutions, pulse profiles, suitability for high-precision timing work, and the retrospective survey efficiency (§6).

2. RADIO SEARCH CAMPAIGN

Targeted observations of LAT sources were conducted over several iterations of the observing program P814 with the 64-m Parkes radio telescope (now *Murriyang*¹). Kerr et al. (2012) report results from an initial survey of sources in the 1FGL γ -ray source catalog (Abdo et al. 2010), while Camilo et al. (2015) discuss searches of 2FGL sources and consider detection statistics. Further searches based on a preliminary version of the 4FGL (Abdollahi et al. 2020) catalog were conducted from 2015 to 2017. As with previous searches, these sources were selected by their lack of association with other known source classes; their lack of variability; and a spectral shape similar to those of other pulsars, viz. a

power law with a cutoff at roughly 1 GeV; see Camilo et al. (2015) for more details. All data taken in 2015 and 2016, on 65 unique targets, were reduced soon after observation and were searched for pulsation as described in Kerr et al. (2012) and Camilo et al. (2015). The final data, from 2017, included 15 new targets that were processed recently, as described below.

All observations were carried out at 20 cm using the DFB4 backend at a center frequency of 1369 MHz with 256 MHz of bandwidth filtered into 512-channel total-power spectra recorded every 80 μ s. From October 2015 through March 2016, we used the multi-beam receiver. We used the H-OH receiver for the remainder of 2016, and we resumed use of the multi-beam receiver in 2017. Observations were typically one hour in duration, with shorter observations filling schedule gaps. The target names (which reflect the position), precise pointing information, observation dates, and integration times are available in Appendix A. Here, we summarize the observing program and discoveries.

In 2015, 13 targets were observed, most more than once. PSR J1833–3840 was discovered in the first attempt on 2015 October 17, and was later confirmed in a short observation with the Green Bank Telescope.

In the second half of the semester, February and March of 2016, 14 additional new targets were observed, and PSR J1803–4719 was discovered in the first observation of the source, on 2016 February 3. PSR J0646–5455 was discovered in a 60-minute observation carried out on 2016 March 28². The pulsar had not been detected in two February observations of 30- and 60-minute duration, likely due to scintillation.

In the first half of the October 2016 semester, we observed 38 new targets. Most sources were observed only once, for one hour. PSR J2045–6837 was discovered on 2016 November 6.

Finally, in February of 2017, we observed 15 new targets. We reduced those data using PRESTO (Ransom 2001) as follows: we used `rfifind` to identify radio frequency interference (RFI) and blank the affected time and frequency bins; we divided data into 8 sub-bands and dedispersed them into time series with trial DMs ranging from 0 to 500 pc cm⁻³; and we performed an `accelsearch` with `zmax`= 200 and summing up to 8 harmonics. We did not find any additional pulsar candidates, though some of these targets are now known to be pulsars (see §6.6).

3. RADIO TIMING CAMPAIGN

In a typical follow-up campaign to obtain a pulsar timing solution, observations are scheduled with a quasi-logarithmic spacing, e.g. at separations of 0.5 d, 1 d, 2 d etc., saturating at a monthly monitoring cadence. With

¹ “Skyworld” to the Wiradjuri people.

² PSR J0646–5455 and PSR J2045–6837 may be the first and only pulsars discovered with the H-OH receiver.

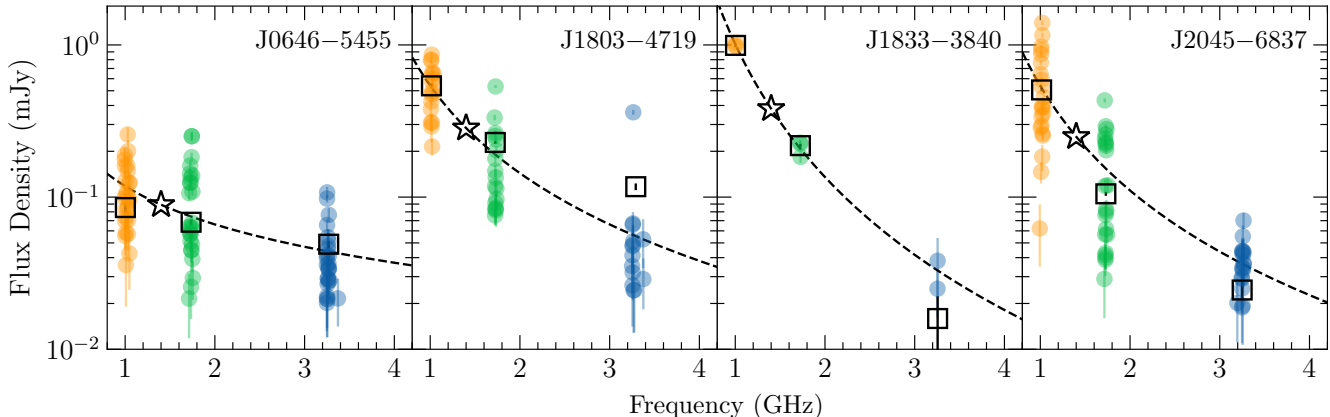


Figure 1. Colored points give the measured flux density for each UWL epoch, with fold mode measurement preferred when available. The sub-bands are centered on 1.0 GHz (orange), 1.7 GHz (green), and 3.3 GHz (blue). The dashed line indicates the best-fit power-law flux model to the mean flux densities, with the black stars using this model to estimate the flux density at the canonical 1.4 GHz. The black squares give the mean flux density for the fold-mode data only—i.e. just for latter epochs—and are shown here for comparison because these observations are used to estimate the timing precision (see Table 1 and §6.5).

this bootstrap approach, the measured and required precisions on parameters like ν increase at roughly the same rate. The goal is to predict the pulse phase at the next observing epoch to within at most a few neutron star rotations (wraps). As the data span lengthens, parameters like the spindown ($\dot{\nu}$) and position become measurable. Binarity complicates the picture, especially if the orbital period has a similar timescale to other parameters. With about one year of data, it is generally possible to obtain a good timing solution, historically by inspired guessing of the number of wraps between observing epochs.

More recent methods aim to systematize and automate this guessing procedure (Freire & Ridolfi 2018; Phillips & Ransom 2020; Taylor et al. 2024). Even with such automated tools, a timing solution can be difficult to obtain in practice. It may not be possible to schedule observations optimally, and—due to scintillation, eclipses, radio-frequency interference (RFI), or telescope outages—some epochs may not yield a pulsar detection. Obtaining a unique timing solution using brute force methods rapidly becomes intractable with sparse data.

All four MSPs were observed both with residual P814 time and under the auspices of P789, a catch-all program for follow-up timing of MSPs (e.g. Spiewak et al. 2020). Observations were carried out at a typical frequency of 1.4 GHz and a length of 30–60 minutes. Due to their later discovery, the coverage for J0646–5455 and J2045–6837 was insufficient to yield a timing solution. And while more than 30 epochs for J1803–4729 and J1833–3840 were obtained, there were too few optimally-spaced epochs to obtain a timing solution using available methods at the time.

To aid the process of obtaining a unique timing position, we observed one of the new MSPs, PSR J2045–6837, with MeerKAT using the *L*-band

(856–1712 MHz) receiver for 10 minutes on 24 August 2021 and 31 August 2021, using the FBFUSE and AP-SUSE instruments to form and record coherent tied-array total-intensity beams. In the first observation, we formed 480 beams covering the *Fermi* localization region, and searched these for pulsations around the known DM using the *Peasoup* pulsar searching software (Barr 2020). In the second observation, we used a denser tiling of 27 beams around the position of the brightest detection from the first observation. The pulsar was detected in 23 out of 27 of these beams with a peak signal-to-noise ratio exceeding 80. From these detections on the second epoch, we obtained an interferometric position with approximate $1''$ uncertainties using the *SeeKAT* software (Bezuidenhout et al. 2023).

While preparing the proposal for what would become P1229, we attempted to solve these pulsars again. We were able to obtain a timing solution for J1833–3840 using new automated tools (Phillips & Ransom 2020; Taylor et al. 2024) and subsequently detected γ -ray pulsations (Smith et al. 2023). Consequently, we only observed three MSPs for P1229 in a one-year campaign beginning in November 2023.

For P1229, we used the Ultra Wide-bandwidth Low (UWL, Hobbs et al. 2020) receiver to collect coherently dedispersed search-mode data over the 704–4032 MHz band, sampling 3328-channel total power spectra every $64 \mu\text{s}$. Typical observations were one hour in length, and in some cases we observed the pulsed noise diode calibration source beforehand. Once we obtained initial timing solutions (see below), we began to collect simultaneous search- and fold-mode data, the latter having 1024 phase bins and all four Stokes parameters.

3.1. *PRESTO* analysis

We reduced the data in two different ways. We processed all search mode data with *PRESTO* (Ransom

2001), using `rfifind` for RFI mitigation; `prepdata` to produce barycentered time series; and `accelsearch` to identify candidate pulsed signals near the known rotation frequencies. We folded the observations with detections and extracted pulse times-of-arrival (TOAs) with a simple gaussian template. We did this for each of three sub-bands (see §3.2). We reduced the archival DFB4 timing data in the same way but did not further divide the 256 MHz bandwidth.

To obtain timing solutions, we developed a new technique building on the approaches of Freire & Ridolfi (2018), Phillips & Ransom (2020) and Taylor et al. (2024) but exploiting the correlations between phase wraps and timing model parameters to avoid expensive timing-model evaluations, and incorporating prior information to reduce the search space, speeding up the phase-connecting process by several orders of magnitude (Clark, C. J. and van Haasteren, R., in prep.). We further improved on this by adopting lattice reduction techniques, inspired by Gazith et al. (2024). With this approach, we obtained timing solutions to all three MSPs. While the solutions for PSRs J1803–4719 and J2045–6837 were unambiguous, the radio TOAs for J0646–5455 yielded several candidate phase-connected timing solutions with different rotation counts between widely separated TOAs. Only one of these yielded γ -ray pulsations when we used it to fold the *Fermi*-LAT data. With these timing solutions, we used `PRESTO` to produce a final set of TOAs using multi-gaussian models of the pulse profiles. These are the radio TOAs used for all timing solutions.

3.2. *psrchive* analysis

To obtain calibrated flux density measurements and detailed pulse profiles, we used `psrchive` (Hotan et al. 2004). First, we folded the search mode data using `dspsr` (van Straten & Bailes 2011). We then processed the folded profiles and the native fold-mode data using a pipeline (Johnston et al. 2021) developed for the Parkes young pulsar timing program P574 (Weltevrede et al. 2010). During this step, polarization and flux calibration are applied. For most epochs, we have at least one contemporary observation of the calibration source, while for a few, we use the nearest-in-time calibrator. The UWL gains are stable for weeks, but change substantially after a system reset. We checked that the epochs with missing calibrators appeared to be in a stable phase well represented by the close-in-time calibration solution.

We further split the calibrated data into three sub-bands covering the frequency ranges 704–1216 MHz, 1216–2240 MHz, and 2496–4032 MHz, excluding the two 128 MHz sub-bands near the 2.4 GHz WiFi band due to severe RFI contamination. Each of the remaining bands is also affected by RFI, which we manually excise, with roughly 50%, 30%, and 15% of the frequency-time samples in a typical observation lost.

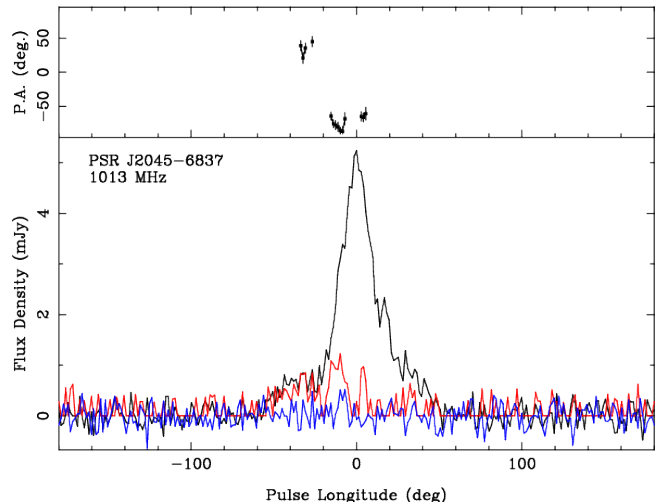


Figure 2. The polarization properties of PSR J2045–6837 in the low-frequency sub-band. The black, red, and blue traces gives Stokes I, $L = U + Q$, and V, respectively. The left shoulder appears to be nearly 100% linearly polarized, allowing measurement of the polarization position angle (P.A.) for some phase bins.

We built a single analytic model of the pulse profile for each pulsar by fitting multiple gaussian components to a single high-S/N observation from the mid-frequency sub-band. Using the calibrated profiles, this standard pulse profile model, and the `psrflux` tool, we computed the flux density S_ν in each sub-band at each epoch. We discarded epochs with a fractional uncertainty >0.33 and show the resulting values in Figure 1. We fit a power-law model, $S_\nu = S_{1400} (\nu/1400 \text{ MHz})^\alpha$, to these data and report the best-fit parameters in Table 1.

We used the timing solutions to co-add the fold-mode data and produce higher S/N pulse profiles. With these, we searched for evidence of frequency-dependent polarization rotation in the ISM with the `rmfit` tool. Only PSR J2045–6837 had detectable linear polarization, and we measured rotation measure $RM = 17 \pm 3 \text{ rad m}^{-2}$. The de-rotated, frequency-averaged polarization profile appears in Figure 2.

4. γ -RAY ANALYSIS

We used Pass 8 (Atwood et al. 2013; Bruel et al. 2018) data collected from MJD 54682–60562 (16.1 yr) with reconstructed positions lying within 3° of the pulsar positions and with reconstructed energies ranging from 100 MeV to 30 GeV. To enhance the precision of the timing analysis (Bickel et al. 2008; Kerr 2011), we used the 4FGL-DR4 (Ballet et al. 2023) sky model to compute photon weights, i.e. the probability that each photon originates from the pulsar. We used the radio-data only timing solutions as input and analyzed the data with a

Table 1. Timing and γ -ray Spectral Parameters for the Discovered MSPs

Timing Parameters	PSR J0646–5455	PSR J1803–4719	PSR J1833–3840	PSR J2045–6837
Fermi-LAT 4FGL Source	J0646.4–5455	J1802.8–4719	J1833.0–3840	J2045.9–6835
Right Ascension (J2000)	06 ^h 46 ^m 14 ^s .62993(7)	18 ^h 03 ^m 00 ^s .974(3)	18 ^h 33 ^m 04 ^s .58231(9)	20 ^h 45 ^m 40 ^s .0623(2)
Declination (J2000)	−54°55′14″.103(1)	−47°19′08″.319(9)	−38°40′46″.072(5)	−68°37′26″.158(1)
Pulsar Period (ms)	2.5073	3.6694	1.8661	2.9623
Period Derivative, \dot{P} (10^{-20} s s ^{−1})	0.18122(8)	3.437(1)	1.7770(4)	1.2802(9)
Period Reference Epoch (MJD)	57523.000	57419.974	57549.349	60263.605
Dispersion Measure (pc cm ^{−3})	40.2289(6)	41.642(2)	78.6606(9)	21.0717(6)
Proper motion in RA $\mu_\alpha \cos \delta$ (mas yr ^{−1})	4.3(2)	−1.5(5)	−5(2)	16(2)
Proper motion in Dec μ_δ (mas yr ^{−1})	2.2(2)	−3(2)	−5(3)	−20(3)
Position Reference Epoch (MJD)	60267.86	60222.95	57549.35	60379.90
Orbital Period (days)	9.618521110(3)	90.44184836(9)	0.900452049(8)	5.71727490(1)
Projected Semi-Major Axis (lt-s)	6.551460(2)	34.430149(3)	0.061478(3)	3.978860(2)
Orbital Eccentricity (10^{-5})	3.50(3)	8.96(2)	10(8)	1.37(10)
Epoch of Ascending Node (MJD)	60271.1388002(3)	57419.993662(2)	57311.052610(6)	60263.6049804(7)
Timing-Derived Parameters				
Mass Function ($10^{-3} M_\odot$)	3.26	5.36	3.08×10^{-4}	2.07
Minimum Companion Mass (M_\odot)	≥ 0.198	≥ 0.238	≥ 0.00828	≥ 0.168
DM-derived Distance (YMW16, kpc)	0.37	1.2	4.7	1.3
DM-derived Distance (NE2001, kpc)	1.8	1.2	2.1	0.82
Spin-down Luminosity, \dot{E} (10^{34} erg s ^{−1})	0.4539	2.746	10.80	1.944
Transverse velocity (km s ^{−1})	8.4(4)	19(8)	160(46)	153(14)
Corrected \dot{P} (10^{-20} s s ^{−1})	0.190(4)	3.40(1)	1.63(6)	0.7(2)
Corrected \dot{E} (10^{34} erg s ^{−1})	0.48(1)	2.721(8)	9.9(3)	1.1(3)
Radio Emission Properties				
Rotation Measure (RM) (rad m ^{−2})	17(3)
Flux Density at 1010 MHz (mJy)	0.11(5)	0.5(2)	1.00(2)	0.5(3)
Flux Density at 1730 MHz (mJy)	0.09(6)	0.2(1)	0.21(2)	0.15(11)
Flux Density at 3260 MHz (mJy)	0.04(2)	0.06(8)	0.03(1)	0.04(1)
Flux Density at 1400 MHz (mJy), S_{1400}	0.09(3)	0.3(1)	0.38(2)	0.25(11)
Spectral Index, α	−0.8(6)	−1.9(10)	−2.9(1)	−2.3(6)
TOA Precision at 1010 MHz (μ s)	13	6.4	2.5	4.3
TOA Precision at 1730 MHz (μ s)	5.5	9.9	3.0	15
TOA Precision at 3260 MHz (μ s)	6.8	18	25	27
γ -ray Spectral Properties				
Peak Energy, E_p (GeV)	2.0(2)	0.5(4)	1.3(4)	2.2(3)
Spectral Curvature, d_p	1.3(3)	0.3(3)	0.6(3)	1.2(3)
Photon Index at 100 MeV, Γ_{100}	0.3(4)	1.7(4)	1.2(4)	0.4(4)
Energy Flux, G_{100} (10^{-12} erg cm ^{−2} s ^{−1})	2.7(3)	3.1(7)	2.7(4)	2.4(3)
Efficiency	0.009(4)	0.019(9)	0.07(3)	0.04(2)

NOTE—Numbers in parentheses represent $1\text{-}\sigma$ uncertainties in the last digit as determined from the timing pipeline described in the main text. For the sake of legibility, we truncate the precision of some parameters: exact values are available in the online ephemerides. Minimum companion masses were calculated assuming a pulsar mass of $1.4 M_\odot$. The gamma-ray spectral parameters are from 4FGL-DR4 (Ballet et al. 2023) using a PLEC4 model with $b=0.67$. We have converted these parameters to the more physical quantities identified in 3PC, namely the energy at which the spectral energy density peaks, E_p , the logarithmic curvature d_p evaluated at E_p ; and the logarithmic slope at 100 MeV, Γ_{100} . γ -ray efficiency is estimated as $4\pi G_{100} d^2 / \dot{E}$; this simple formulation assumes that the γ -ray beams illuminate the sky uniformly. All distance-dependent quantities are calculated using the YMW16 (Yao et al. 2017) electron density model and, where needed, assuming 30% uncertainty. NE2001 (Cordes & Lazio 2002) model distances are reported for comparison. The flux density measurements are reported as the mean and standard deviation of all data, while the TOA precision estimates are based only on the limited subset of fold-mode data (see Figure 1).

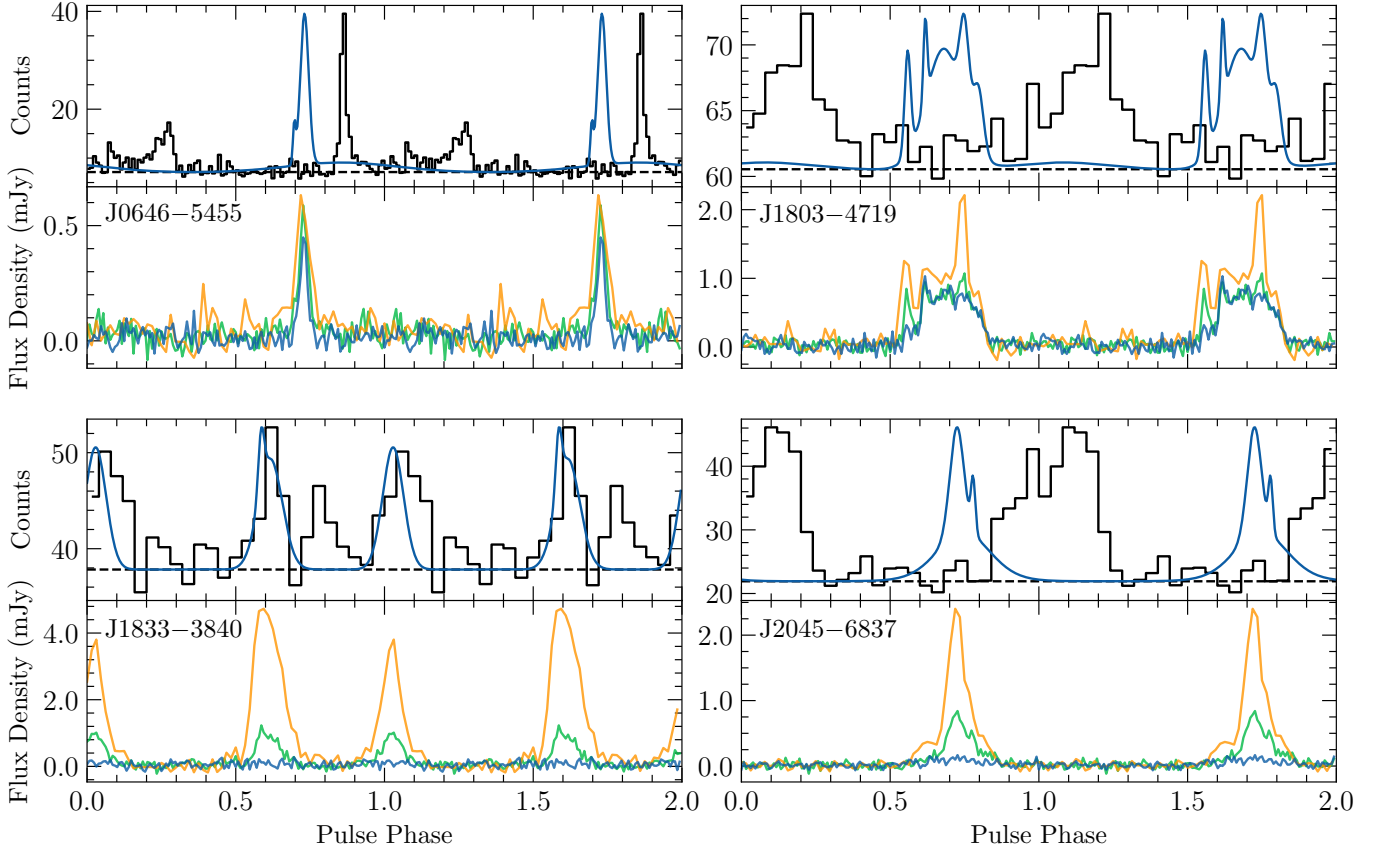


Figure 3. Phase-aligned γ -ray and radio pulse profiles. The top panels for each pulsar show histograms of the LAT photon weights, viz. the γ -ray pulse profiles, with the dashed black line indicating the estimated background level (see [Smith et al. 2023](#)). The smooth blue curve shows the analytic radio template for reference. The bottom panels for each pulsar show the Stokes I pulse profile for the co-added fold-mode data acquired in each of the three sub-bands: yellow is 704–1216 MHz, green is 1216–2240 MHz, and blue is 2496–4032 MHz.

γ -ray pulsar timing pipeline described further in Ajello et al. (2022).

For this work, we implemented a new capability in the γ -ray timing pipeline: in addition to the unbinned Poisson likelihood, we use informative gaussian priors provided by the central values and $1\text{-}\sigma$ uncertainties from the radio ephemeris. The resulting timing solution thus includes all available constraints, remains consistent with the radio TOAs, and benefits from the much longer time span of the γ -ray data. This long observing span t is especially effective in determining parameters whose effects accumulate over time, like proper motion ($\propto t$) and $\dot{\nu}$ ($\propto t^2$).

In the case of PSR J1803–4719, the γ -ray source is faint and the extensive P814 radio data allow good measurement of position, Keplerian, and spin-down parameters. Consequently we report the results of radio-only timing. Conversely, for PSR J0646–5455 and PSR J2045–6837, the posterior is dominated by the γ -ray data. For all four pulsars, the best timing solutions are given in Table 1 and provided in the online material³. We used these timing solutions to fold the γ -ray data and, accounting for dispersion and light travel time, prepared the joint γ -ray and radio pulse profiles shown in Figure 3.

The spectral properties of the γ -ray sources are available in the 4FGL catalog, and we report in Table 1 the relevant spectral parameters from a power-law exponential cutoff model (see 3PC for an extensive discussion). PSR J0646–5455 and J2045–6837 have relatively typical γ -ray MSP spectra, with a d_p (see caption of Table 1 for a definition) value approaching the limit of 4/3 for monoenergetic curvature radiation (see 3PC). On the other hand, the spectrum of PSR J1803–4719 is unusually soft. Given an estimate of distance from the DM using the model of Yao et al. (2017), we obtain γ -ray efficiencies of 1–7%, substantially below the typical values of the MSP population reported in 3PC. We discuss this further below.

5. OTHER WAVELENGTHS

5.1. X-rays

The fields of all four MSPs have been observed with the XRT (Burrows et al. 2005) on the Neil Gehrels Swift observatory with the following livetimes: J0646–5455, 0.8 ks in one ObsID; J1803–4719, 3.4 ks in 8 ObsIDs; J1833–3840, 7.2 ks in 12 ObsIDs; and J2045–6837 for 4.7 ks in 13 ObsIDs. We examined the resulting images and, within the 18" half-power diameter of the XRT point-spread function, found respectively 0, 0, 1, and 2 events. These rates are consistent with the expected background levels. Detecting a potential X-ray coun-

terpart will thus require longer observation with a more sensitive X-ray telescope.

5.2. Optical

The MSP fields are not in the footprints of any of the deep southern sky surveys, and there are no counterparts listed in the third Gaia data release (Gaia Collaboration et al. 2023). For white dwarfs, this catalog is substantially complete only to about 100 pc (Tremblay et al. 2024), much closer than the DM distances for any of the systems. It is perhaps more surprising that the high- \dot{E} black widow J1833–3840 remains undetected given similar (though closer) systems with optical magnitudes <20 . However, we modeled the predicted r-band magnitude using Icarus (Breton et al. 2012), assuming an inclination of 60° , a pulsar mass of $1.6M_\odot$, 25% irradiation efficiency, and with the companion star filling its Roche lobe. The resulting companion temperature peaks at 4300 K on the day side, and at the DM distance, gives a peak magnitude of $r=22.6$, well fainter than the Gaia limiting magnitude.

6. DISCUSSION

Before synthesizing the results of the survey, we first discuss some interesting aspects of each of the new pulsars.

6.1. PSR J0646–5455

This pulsar has by far the highest γ -ray signal-to-noise in the sample, concordant with a DM-estimated distance of only 0.4 kpc. However, with this proximity, the measured efficiency is $<1\%$, one of the lowest values ever measured for a γ -ray MSP. The implied tangential velocity is well constrained and small: 8.4 ± 0.4 km/s. Taken together, these two anomalies suggest that the distance may be underestimated, and indeed the NE2001 implied distance is 1.8 kpc, the largest discrepancy with YMW16 model distances in the sample. (See Olszanski et al. (2025) for a recent discussion of differences between these two models.) Moreover, with $S_{1400} < 100 \mu\text{Jy}$, PSR J0646–5455 is one of the radio-faintest known γ -ray pulsars, though its flux lies above the $30 \mu\text{Jy}$ “radio-faint” threshold adopted by the LAT team (Abdo et al. 2013; Smith et al. 2023). Although radio and γ -ray fluxes are not necessarily correlated (Smith et al. 2023), this low radio flux is also suggestive of a greater distance. Confirming such a low efficiency would provide a valuable constraint on models of γ -ray emission (see Philippov & Kramer 2022), motivating a future parallax measurement. (The precision of parallax measurements with LAT pulsar timing is generally too low to be useful.)

PSR J0646–5455 has a canonical Vela-like pulse profile, with two caustic-shaped γ -ray peaks separated by about $\Delta = 0.4$ and trailing a narrow radio peak by about $\delta = 0.1$ (see 3PC), further indicating that this configu-

³ <https://fermi.gsfc.nasa.gov/ssc/data/access/lat/ephems/>

ration is common across orders of magnitude in \dot{E} , light cylinder size, and magnetic field strength.

The γ -ray brightness, along with a 2.5 ms spin period and narrow pulse profile, make this pulsar suitable for high-precision timing. Following the methods of Ajello et al. (2022), we obtained a single-pulsar gravitational wave background upper limit (95% confidence) of $\mathcal{A}_{\text{gwb}} < 1.3 \times 10^{-13}$, making J0646–5455 one of the 25 best-timed pulsars in the GPTA.

6.2. PSR J1803–4817

PSR J1803–4817 is in the most eccentric binary of the four, and like the other two non-eclipsing systems, the residual eccentricity ($e = 0.9 \times 10^{-4}$) is roughly consistent with the predictions from tidal circularization due to coupling with convective cells in the companion envelope (Phinney 1992), $\epsilon \sim 1.5 \times 10^{-4}(P_b/100 \text{ d}) \approx 1.4 \times 10^{-4}$. Though there is a modest correlation between spin period and orbital period observed in cataloged MSPs, the 3.7 ms spin period is not unusually fast compared to similarly-wide binaries in the Galactic field.

6.3. PSR J1833–3840

PSR J1833–3840 is the only eclipsing pulsar in the sample, and with a minimum companion mass $< 0.01 M_\odot$, it is a black widow. It has an unusually steep spectrum, with an index of nearly -3 , which may be a hallmark of some high- \dot{E} MSPs (e.g. Backer et al. 1982; Fruchter et al. 1988). Indeed, Frail et al. (2018) independently noted this source as a good MSP candidate due to its steep spectrum.

J1833–3840 is also a high- \dot{E} pulsar, and although the γ -ray light curve suffers from a poor S/N, it is clear that the γ -ray emission is largely aligned with the radio peaks, which is also the case for both the original MSP and the original black widow pulsar (Guillemot et al. 2012). It has been suggested (e.g. Bangale et al. 2024) that spider pulsars have faster periods than the isolated and/or less compact systems; with a period of only 1.87 ms, this pulsar provides further support. This low spin period, along with a relatively low surface magnetic field, invite comparison to PSR J0952–0607, a soft radio spectrum, fast-spinning black widow. Modeling of the optical light curve of the heated companion of PSR J0952–0607 suggests a heavy neutron star (Romani et al. 2022), motivating optical follow-up of J1833–3840.

Finally, J1833–3840 has the longest period of any known black widow system and thus gives insight into the evolution of compact, eclipsing binaries. Studies differ as to whether black widows and redbacks (with similar orbital period but companion masses of order $0.1 M_\odot$) are discrete populations (Chen et al. 2013) or consecutive evolutionary phases, with redbacks evolving into black widows (Misra et al. 2024). In the latter scenario, forming a binary with $P_b = 0.9 \text{ d}$ would require

extremely efficient evaporation of the companion. Characterization of the companion elemental abundance and other properties strengthen constraints on the binary evolution, further motivating optical studies.

6.4. PSR J2045–6837

With a proper motion of $25 \pm 2 \text{ mas yr}^{-1}$, the implied spatial velocity at the DM distance of 1.3 kpc is $152 \pm 14 \text{ km s}^{-1}$, about twice the mean two-dimensional speed observed for recycled pulsars (Hobbs et al. 2004). The γ -ray efficiency, about 4%, is also relatively low. These anomalies are modest, but can be alleviated if the true distance to the pulsar is $< 1 \text{ kpc}$, as is the case for the NE2001 model distance. Alternatively, if the high spatial velocity is confirmed, it would provide a useful datum for the strength of supernova kicks relative to requirements for binary disruption.

PSR J2045–6837 has a steeper-than-average radio spectrum, and the leading edge of its pulse profile is highly polarized (Figure 2), enabling the only measurement of RM for the sample.

6.5. Suitability for Radio PTAs

We give a rough estimate of the typical radio timing precision for these pulsars with the *Murriyang* UWL in Table 1 but provide more context here. These measurements are based only on the fold-mode data, which is limited. In particular, some of the brightest epochs for PSR J0646–5455 were observed only in “search-mode”, so that the reported timing precision is conservative. PSR J1833–3840 could reliably deliver timing precision at the $2\text{--}3 \mu\text{s}$ level (in one hour) and, due to the larger DM, is less subject to scintillation. The other pulsars are too faint to time with high precision without dynamic scheduling to target scintillation maxima. On the other hand, given the relatively steep spectra for all pulsars save PSR J0646–5455—and especially that of the eclipsing J1833–3840—MeerKAT and the future SKA (both Mid and Low) should regularly achieve μs -precision measurements for these pulsars, making them plausible PTA candidates.

6.6. The Survey in Retrospect

Targeting pulsar-like LAT sources has yielded good return on telescope time investment. Early surveys with the GBT at 820 MHz (Ransom et al. 2011) and 350 MHz (Bangale et al. 2024) had a purity of $3/25=12\%$ and $18/49=37\%$, respectively⁴. Meanwhile, early surveys with the Parkes observatory had $2/11=18\%$ (Keith et al. 2011), $5/14=36\%$ (Kerr et al. 2012) purity. After these

⁴ Because it was published well after the survey completion, Bangale et al. (2024) provided a careful analysis of subsequent discoveries in their target list, as we have here. For other surveys, only the initially reported number of MSP discoveries is considered.

Table 2. Pulsars Discovered in Survey Targets

Target	Pulsar	Telescope/Survey
J0312–0920	J0312–0921	GBT
J0744–2435	J0744–2525 [†]	E@H
J0838–2827	J0838–2827	TRAPUM ^{T24}
J0952–0608	J0952–0607	LOFAR ^{B17}
J0646–5455	J0646–5455	this work
J1204–5033	J1207–5050	GMRT ^{B21}
J1208–6238	J1208–6238 [†]	E@H
J1259–8149	J1259–8148	TRAPUM
J1304+1203	J1304+12	AO
J1335–5656	J1335–5656	E@H
J1345–2612	J1346–2610	TRAPUM
J1544–2534	J1544–2555	TRAPUM
J1555–2908	J1555–2908	GBT ^{R22}
J1611–6011	J1603–6011	TRAPUM
J1623–6935	J1623–6936	TRAPUM ^{C23}
J1649–3010	J1649–3012	E@H
J1653–0158	J1653–0158	E@H ^{N20}
J1802–4718	J1803–4719	this work
J1823–3543	J1823–3543	TRAPUM ^{C23}
J1832–3840	J1833–3840	this work
J1858–5425	J1858–5422	TRAPUM ^{C23}
J2029–4237	J2029–4239	TRAPUM
J2045–6835	J2045–6837	this work

NOTE— Now-known MSPs and young pulsars[†] associated with the pulsar search targets. Information about unpublished pulsars is available from the Galactic MSP list at <https://www.astro.umd.edu/~eferrara/pulsars/GalacticMSPs.txt> and the Einstein@Home website, https://einsteinathome.org/gammaraypulsar/FGRP1_discoveries.html. References: (B17) Bassa et al. (2017) (N20) Nieder et al. (2020) (B21) Bhattacharyya et al. (2021) (R22) Ray et al. (2022) (C23) Clark et al. (2023) (T24) Thongmeekom et al. (2024).

initial successes, there was some indication of diminishing returns. Camilo et al. (2015) reported the detection of 11/56=20% new pulsars, but these included the discoveries of Kerr et al. (2012); the new 2FGL targets only yielded 6/42=14% purity. Using the Effelsberg telescope, Barr et al. (2013) searched 289 LAT targets based on 1FGL and found only 1 MSP. In this work, we report only 4 discoveries from 80 4FGL-based targets, for a comparatively low 5% success rate.

However, in the years since these original discoveries were made, the sources have been searched with other telescopes, and 17 more MSPs and 2 young pulsars have been found, as listed in Table 2. Five of these are radio-quiet pulsars discovered in direct searches of the LAT data with Einstein@Home (e.g. Clark et al. 2018). A further two targets are likely to be pulsars: J0523–2527 is a high-confidence compact binary (redback) candidate (Strader et al. 2014) while J1120–2214 is an optical NS-proto WD system that also likely hosts a pulsar (Swihart et al. 2022).

For the radio-loud pulsars, a common feature for successful detection is the use of a more sensitive or lower-

frequency telescope. And indeed, the pulsars discovered in this survey are generally not very radio bright, with PSR J0646–5455 having a mean flux density at 1.4 GHz well below 0.1 mJy; this is a typical sensitivity threshold for a radio survey. The remaining three pulsars all have relatively steep spectra and are indicative of the pulsars well-suited for low-frequency observations. Finally, repeated observations also play an important role. Because it is observable at a favorable local sidereal time range and because of its quality as a pulsar candidate, we observed J0838–2827 no fewer than 11 times, with no detections. The TRAPUM team were able to discover pulsations with MeerKAT (Thongmeekom et al. 2024), but nonetheless required many additional attempts to verify the discovery detection of this extremely enshrouded redback.

When considering these subsequent pulsar detections, the target selection increases to 29% purity, indicating that relatively faint, new sources in 4FGL continue to provide excellent targets for radio telescopes.

We can draw a few more conclusions from this analysis. First, the surveys which used manually-curated target lists (Bangale et al. (2024), Kerr et al. (2012), and this work) tend to have the highest purity, although classification with earlier machine learning techniques (e.g. Saz Parkinson et al. 2016) has also been successful. Conversely, Barr et al. (2013) cast a very wide net, observing nearly half of the 600 unidentified sources in the 1FGL catalog, of which the majority are likely blazars. Moreover, many of the targets of Barr et al. (2013) were in the Galactic plane. While this is a natural choice when looking for pulsars, the analysis techniques for γ -ray sources at low Galactic latitude have advanced substantially since 1FGL, and Barr et al. (2013) noted that many of their targets were absent or had moved more than the telescope beam size when compared to 2FGL. While Galactic γ -ray source positions are likely now more reliable, it remains true that targeting higher Galactic latitudes also targets the relatively nearby MSP population to which LAT is most sensitive.

On the other hand, it may be that accepting lower survey efficiency will be necessary for improved understanding of the γ -ray MSP population. The new MSPs reported here all have γ -ray efficiencies well below the mean reported in 3PC. It is possible that these efficiencies are in error (e.g. all of the DM distance estimates are too low). But it is also possible that the discoveries of these pulsars are beginning to correct a bias in the LAT population, which was established largely through search efforts like the one described here. Those are naturally biased towards the brightest sources, which can be bright both by being close and by being particularly efficient, either through favorable beaming or a truly high γ -ray luminosity. Quantifying the full spread of the range of MSP efficiencies is key both to understanding their magnetospheres and the production of γ rays (e.g. Philippov & Kramer 2022) and to determining the con-

tribution of MSP populations to features like the Fermi Galactic center excess (e.g. [Ackermann et al. 2017](#)).

1 We thank Lawrence Toomey for assistance in wrangling
2 the data and Jane Kaczmarek for help in scheduling filler
3 observations which helped in obtaining phase connec-
4 tion.

5 The *Fermi* LAT Collaboration acknowledges gener-
6 ous ongoing support from a number of agencies and
7 institutes that have supported both the development
8 and the operation of the LAT as well as scientific data
9 analysis. These include the National Aeronautics and
10 Space Administration and the Department of Energy in
11 the United States, the Commissariat à l’Energie Atom-
12 ique and the Centre National de la Recherche Scien-
13 tifique / Institut National de Physique Nucléaire et de
14 Physique des Particules in France, the Agenzia Spaziale
15 Italiana and the Istituto Nazionale di Fisica Nucleare in
16 Italy, the Ministry of Education, Culture, Sports, Sci-
17 ence and Technology (MEXT), High Energy Accelerator
18 Research Organization (KEK) and Japan Aerospace Ex-
19 ploration Agency (JAXA) in Japan, and the K. A. Wal-
20 lenberg Foundation, the Swedish Research Council and
21 the Swedish National Space Board in Sweden.

22 Additional support for science analysis during the op-
23 erations phase is gratefully acknowledged from the Is-
24 tituto Nazionale di Astrofisica in Italy and the Cen-
25 tre National d’Études Spatiales in France. This work
26 performed in part under DOE Contract DE-AC02-
27 76SF00515.

28 Murriyang, the Parkes radio telescope, is part of the
29 Australia Telescope National Facility, which is funded by
30 the Australian Government for operation as a National
31 Facility managed by CSIRO.

32 Work at NRL is supported by NASA, in part by Fermi
33 Guest Investigator grant NNG22OB35A.

34 The MeerKAT telescope is operated by the South
35 African Radio Astronomy Observatory, which is a fa-
36 cility of the National Research Foundation, an agency
37 of the Department of Science and Innovation.

38 Observations used the FBFUSE and APSUSE com-
39 puting clusters for data acquisition, storage and anal-
40 ysis. These clusters were funded, designed and in-
41 stalled by the Max-Planck-Institut-für-Radioastronomie
42 (MPIfR) and the Max-Planck-Gesellschaft. FBFUSE
43 performs beamforming operations in real-time using the
44 *mosaic*⁵ software stack ([Chen et al. 2021](#)).

Facilities: Fermi

REFERENCES

- Abdo, A. A., Ackermann, M., Ajello, M., et al. 2010, *ApJS*,
188, 405, doi: [10.1088/0067-0049/188/2/405](https://doi.org/10.1088/0067-0049/188/2/405)
- Abdo, A. A., Ajello, M., Allafort, A., et al. 2013, *ApJS*,
208, 17, doi: [10.1088/0067-0049/208/2/17](https://doi.org/10.1088/0067-0049/208/2/17)
- Abdollahi, S., Acero, F., Ackermann, M., et al. 2020, *ApJS*,
247, 33, doi: [10.3847/1538-4365/ab6bcb](https://doi.org/10.3847/1538-4365/ab6bcb)
- Ackermann, M., Ajello, M., Albert, A., et al. 2017, *ApJ*,
840, 43, doi: [10.3847/1538-4357/aa6cab](https://doi.org/10.3847/1538-4357/aa6cab)
- Ajello, M., Atwood, W. B., Baldini, L., et al. 2022, *Science*,
376, 521, doi: [10.1126/science.abm3231](https://doi.org/10.1126/science.abm3231)
- Atwood, W., Albert, A., Baldini, L., et al. 2013, arXiv
e-prints, arXiv:1303.3514, doi: [10.48550/arXiv.1303.3514](https://doi.org/10.48550/arXiv.1303.3514)

- Atwood, W. B., Abdo, A. A., Ackermann, M., et al. 2009, *ApJ*, 697, 1071, doi: [10.1088/0004-637X/697/2/1071](https://doi.org/10.1088/0004-637X/697/2/1071)
- Backer, D. C., Kulkarni, S. R., Heiles, C., Davis, M. M., & Goss, W. M. 1982, *Nature*, 300, 615, doi: [10.1038/300615a0](https://doi.org/10.1038/300615a0)
- Ballet, J., Bruel, P., Burnett, T. H., Lott, B., & The Fermi-LAT collaboration. 2023, arXiv e-prints, arXiv:2307.12546, doi: [10.48550/arXiv.2307.12546](https://doi.org/10.48550/arXiv.2307.12546)
- Bangale, P., Bhattacharyya, B., Camilo, F., et al. 2024, *ApJ*, 966, 161, doi: [10.3847/1538-4357/ad2994](https://doi.org/10.3847/1538-4357/ad2994)
- Barr, E. 2020, Peasoup: C++/CUDA GPU pulsar searching library. <http://ascl.net/2001.014>
- Barr, E. D., Guillemot, L., Champion, D. J., et al. 2013, *MNRAS*, 429, 1633, doi: [10.1093/mnras/sts449](https://doi.org/10.1093/mnras/sts449)
- Bassa, C. G., Pleunis, Z., Hessels, J. W. T., et al. 2017, *ApJL*, 846, L20, doi: [10.3847/2041-8213/aa8400](https://doi.org/10.3847/2041-8213/aa8400)
- Bezuidenhout, M. C., Clark, C. J., Breton, R. P., et al. 2023, *RAS Techniques and Instruments*, 2, 114, doi: [10.1093/rasti/rzad007](https://doi.org/10.1093/rasti/rzad007)
- Bhattacharyya, B., Roy, J., Johnson, T. J., et al. 2021, *ApJ*, 910, 160, doi: [10.3847/1538-4357/abe4d5](https://doi.org/10.3847/1538-4357/abe4d5)
- Bickel, P., Kleijn, B., & Rice, J. 2008, *ApJ*, 685, 384, doi: [10.1086/590399](https://doi.org/10.1086/590399)
- Breton, R. P., Rappaport, S. A., van Kerkwijk, M. H., & Carter, J. A. 2012, *ApJ*, 748, 115, doi: [10.1088/0004-637X/748/2/115](https://doi.org/10.1088/0004-637X/748/2/115)
- Bruel, P., Burnett, T. H., Digel, S. W., et al. 2018, arXiv e-prints, arXiv:1810.11394. <https://arxiv.org/abs/1810.11394>
- Burrows, D. N., Hill, J. E., Nousek, J. A., et al. 2005, *SSRv*, 120, 165, doi: [10.1007/s11214-005-5097-2](https://doi.org/10.1007/s11214-005-5097-2)
- Camilo, F., Kerr, M., Ray, P. S., et al. 2015, *ApJ*, 810, 85, doi: [10.1088/0004-637X/810/2/85](https://doi.org/10.1088/0004-637X/810/2/85)
- Chen, H.-L., Chen, X., Tauris, T. M., & Han, Z. 2013, *ApJ*, 775, 27, doi: [10.1088/0004-637X/775/1/27](https://doi.org/10.1088/0004-637X/775/1/27)
- Chen, W., Barr, E., Karuppusamy, R., Kramer, M., & Stappers, B. 2021, *Journal of Astronomical Instrumentation*, 10, 2150013, doi: [10.1142/S2251171721500136](https://doi.org/10.1142/S2251171721500136)
- Clark, C. J., Pletsch, H. J., Wu, J., et al. 2018, *Science Advances*, 4, eaao7228, doi: [10.1126/sciadv.aao7228](https://doi.org/10.1126/sciadv.aao7228)
- Clark, C. J., Kerr, M., Barr, E. D., et al. 2023, *Nature Astronomy*, 7, 451, doi: [10.1038/s41550-022-01874-x](https://doi.org/10.1038/s41550-022-01874-x)
- Clark, C. J., Breton, R. P., Barr, E. D., et al. 2023, *Monthly Notices of the Royal Astronomical Society*, 519, 5590, doi: [10.1093/mnras/stac3742](https://doi.org/10.1093/mnras/stac3742)
- Cordes, J. M., & Lazio, T. J. W. 2002, ArXiv Astrophysics e-prints
- Frail, D. A., Ray, P. S., Mooley, K. P., et al. 2018, *MNRAS*, 475, 942, doi: [10.1093/mnras/stx3281](https://doi.org/10.1093/mnras/stx3281)
- Freire, P. C. C., & Ridolfi, A. 2018, *MNRAS*, 476, 4794, doi: [10.1093/mnras/sty524](https://doi.org/10.1093/mnras/sty524)
- Fruchter, A. S., Stinebring, D. R., & Taylor, J. H. 1988, *Nature*, 333, 237, doi: [10.1038/333237a0](https://doi.org/10.1038/333237a0)
- Gaia Collaboration, Vallenari, A., Brown, A. G. A., et al. 2023, *A&A*, 674, A1, doi: [10.1051/0004-6361/202243940](https://doi.org/10.1051/0004-6361/202243940)
- Gazith, D., Zackay, B., & Pearlman, A. B. 2024, arXiv e-prints, arXiv:2402.07228, doi: [10.48550/arXiv.2402.07228](https://doi.org/10.48550/arXiv.2402.07228)
- Guillemot, L., Johnson, T. J., Venter, C., et al. 2012, *ApJ*, 744, 33, doi: [10.1088/0004-637X/744/1/33](https://doi.org/10.1088/0004-637X/744/1/33)
- Hobbs, G., Lyne, A. G., Kramer, M., Martin, C. E., & Jordan, C. 2004, *MNRAS*, 353, 1311, doi: [10.1111/j.1365-2966.2004.08157.x](https://doi.org/10.1111/j.1365-2966.2004.08157.x)
- Hobbs, G., Manchester, R. N., Dunning, A., et al. 2020, *PASA*, 37, e012, doi: [10.1017/pasa.2020.2](https://doi.org/10.1017/pasa.2020.2)
- Hotan, A. W., van Straten, W., & Manchester, R. N. 2004, *PASA*, 21, 302, doi: [10.1071/AS04022](https://doi.org/10.1071/AS04022)
- Johnston, S., Sobey, C., Dai, S., et al. 2021, *MNRAS*, 502, 1253, doi: [10.1093/mnras/stab095](https://doi.org/10.1093/mnras/stab095)
- Keith, M. J., Johnston, S., Ray, P. S., et al. 2011, *MNRAS*, 414, 1292, doi: [10.1111/j.1365-2966.2011.18464.x](https://doi.org/10.1111/j.1365-2966.2011.18464.x)
- Kerr, M. 2011, *ApJ*, 732, 38, doi: [10.1088/0004-637X/732/1/38](https://doi.org/10.1088/0004-637X/732/1/38)
- Kerr, M., Camilo, F., Johnson, T. J., et al. 2012, *ApJL*, 748, L2, doi: [10.1088/2041-8205/748/1/L2](https://doi.org/10.1088/2041-8205/748/1/L2)
- Manchester, R. N., Hobbs, G. B., Teoh, A., & Hobbs, M. 2005, *AJ*, 129, 1993, doi: [10.1086/428488](https://doi.org/10.1086/428488)
- Misra, D., Linares, M., & Ye, C. S. 2024, arXiv e-prints, arXiv:2408.16048, doi: [10.48550/arXiv.2408.16048](https://doi.org/10.48550/arXiv.2408.16048)
- Narayan, R. 1992, *Philosophical Transactions of the Royal Society of London Series A*, 341, 151, doi: [10.1098/rsta.1992.0090](https://doi.org/10.1098/rsta.1992.0090)
- Nieder, L., Clark, C. J., Kandel, D., et al. 2020, *ApJL*, 902, L46, doi: [10.3847/2041-8213/abb02](https://doi.org/10.3847/2041-8213/abb02)
- Olszanski, T. E. E., Lewis, E. F., Deneva, J. S., et al. 2025, arXiv e-prints, arXiv:2502.04571, doi: [10.48550/arXiv.2502.04571](https://doi.org/10.48550/arXiv.2502.04571)
- Philippov, A., & Kramer, M. 2022, *Annual Review of Astronomy and Astrophysics*, 60, 495, doi: [10.1146/annurev-astro-052920-112338](https://doi.org/10.1146/annurev-astro-052920-112338)
- Phillips, C., & Ransom, S. 2020, arXiv e-prints, arXiv:2012.07809, doi: [10.48550/arXiv.2012.07809](https://doi.org/10.48550/arXiv.2012.07809)
- Phinney, E. S. 1992, *Philosophical Transactions of the Royal Society of London Series A*, 341, 39, doi: [10.1098/rsta.1992.0084](https://doi.org/10.1098/rsta.1992.0084)
- Polzin, E. J., Breton, R. P., Bhattacharyya, B., et al. 2020, *MNRAS*, 494, 2948, doi: [10.1093/mnras/staa596](https://doi.org/10.1093/mnras/staa596)
- Ransom, S. M. 2001, PhD thesis, Harvard University, Massachusetts

- Ransom, S. M., Ray, P. S., Camilo, F., et al. 2011, *ApJL*, 727, L16, doi: [10.1088/2041-8205/727/1/L16](https://doi.org/10.1088/2041-8205/727/1/L16)
- Ray, P. S., Abdo, A. A., Parent, D., et al. 2012, arXiv e-prints, arXiv:1205.3089, doi: [10.48550/arXiv.1205.3089](https://doi.org/10.48550/arXiv.1205.3089)
- Ray, P. S., Nieder, L., Clark, C. J., et al. 2022, *ApJ*, 927, 216, doi: [10.3847/1538-4357/ac49ef](https://doi.org/10.3847/1538-4357/ac49ef)
- Romani, R. W., Kandel, D., Filippenko, A. V., Brink, T. G., & Zheng, W. 2022, *ApJL*, 934, L17, doi: [10.3847/2041-8213/ac8007](https://doi.org/10.3847/2041-8213/ac8007)
- Saz Parkinson, P. M., Xu, H., Yu, P. L. H., et al. 2016, *ApJ*, 820, 8, doi: [10.3847/0004-637X/820/1/8](https://doi.org/10.3847/0004-637X/820/1/8)
- Smith, D. A., Abdollahi, S., Ajello, M., et al. 2023, *ApJ*, 958, 191, doi: [10.3847/1538-4357/acee67](https://doi.org/10.3847/1538-4357/acee67)
- Spiewak, R., Flynn, C., Johnston, S., et al. 2020, *MNRAS*, 496, 4836, doi: [10.1093/mnras/staa1869](https://doi.org/10.1093/mnras/staa1869)
- Strader, J., Chomiuk, L., Sonbas, E., et al. 2014, *ApJL*, 788, L27, doi: [10.1088/2041-8205/788/2/L27](https://doi.org/10.1088/2041-8205/788/2/L27)
- Swihart, S. J., Strader, J., Aydi, E., et al. 2022, *ApJ*, 926, 201, doi: [10.3847/1538-4357/ac4ae4](https://doi.org/10.3847/1538-4357/ac4ae4)
- Taylor, J., Ransom, S., & Padmanabh, P. V. 2024, *ApJ*, 964, 128, doi: [10.3847/1538-4357/ad1ce9](https://doi.org/10.3847/1538-4357/ad1ce9)
- Thongmeearkom, T., Clark, C. J., Breton, R. P., et al. 2024, *MNRAS*, 530, 4676, doi: [10.1093/mnras/stae787](https://doi.org/10.1093/mnras/stae787)
- Tremblay, P.-E., Bédard, A., O'Brien, M. W., et al. 2024, *NewAR*, 99, 101705, doi: [10.1016/j.newar.2024.101705](https://doi.org/10.1016/j.newar.2024.101705)
- van Straten, W., & Bailes, M. 2011, *PASA*, 28, 1, doi: [10.1071/AS10021](https://doi.org/10.1071/AS10021)
- Weltevrede, P., Johnston, S., Manchester, R. N., et al. 2010, *PASA*, 27, 64, doi: [10.1071/AS09054](https://doi.org/10.1071/AS09054)
- Yao, J. M., Manchester, R. N., & Wang, N. 2017, *ApJ*, 835, 29, doi: [10.3847/1538-4357/835/1/29](https://doi.org/10.3847/1538-4357/835/1/29)

APPENDIX

A. TARGETS

Table 3 gives the full record of pointing positions and integration lengths for Parkes observations made for P814. The “Target” column indicates the name by which data can be found in the CSIRO online archive. For the detected pulsars, we include the search epochs but exclude subsequent timing observations. We also exclude some observations logged with the P814 project code but which were not intended for pulsar searches, e.g. timing of the newly-discovered PSR J1208–6238. NB that this table does not include observations of these targets carried out under other search campaigns, potentially at other telescopes, under the auspices of the Pulsar Search Consortium⁶ (Ray et al. 2012) or otherwise. (See Table 2 for the campaigns which have subsequently discovered pulsations in some of these targets.)

We have compared the pointing positions to the 4FGL-DR4 source catalog and indicate the distance to the nearest source. In most cases, the separation is much less than the size of the telescope beam, about $7'$ radius. Because the target list was based on a preliminary version of the catalog, in a few cases, the targeted source is not in the 4FGL catalog, and when no catalog source exists within 0.3° , no counterpart is listed. Due to a transcription error, an incorrect pointing position was used for (now) PSR J1555–2908, which has a 4FGL counterpart.

Table 3. Pointing Information for Sources Searched

Target	Date	Length (s)	R.A.	Decl.	4FGL-DR4	Separation ($^\circ$)
J0245–5951	2016-11-04	3606	41.37083	-59.85000	J0245.4–5950	0.018
J0312–0920	2016-11-04	3606	48.04583	-9.33806	J0312.1–0921	0.024
	2016-11-06	2393				
	2017-02-13	968				
	2017-02-13	3606				
J0414–4259	2015-10-17	3606	63.70000	-42.98694	J0414.7–4300	0.025
	2015-10-17	4006				
	2015-11-22	3606				
	2015-11-22	5627				
	2016-01-17	3606				
J0443–6651	2016-11-04	3606	70.88333	-66.85556	J0443.3–6652	0.018
J0523–2527	2016-11-04	3606	80.82917	-25.45528	J0523.3–2527	0.008
J0628+0519	2017-02-21	3606	97.18333	5.32139		
	2017-02-22	2706				
J0646–5455	2016-02-03	3606	101.60833	-54.91889	J0646.4–5455	0.010
	2016-03-03	1313				
	2016-03-28	3606				
	2016-03-28	1803				
	2016-03-28	3606				
J0744–2535	2017-02-16	3606	116.04583	-25.39944	J0744.0–2525	0.043
	2017-02-17	3606				
	2017-02-20	3606				
	2017-03-19	3606				
J0745–4028	2017-02-21	3606	116.25000	-40.47111	J0744.9–4028	0.004
J0749+1325	2016-11-05	3597	117.41250	13.43306	J0749.6+1324	0.026
J0754–3953	2015-10-17	3606	118.70833	-39.88694	J0754.9–3953	0.026
	2015-11-22	3606				
	2015-11-22	3606				
	2016-02-03	3606				
	2016-03-28	3606				

Table 3 *continued*

⁶ A substantial but incomplete set of logs for PSC observations is available upon request to the authors.

Table 3 (*continued*)

Target	Date	Length (s)	R.A.	Decl.	4FGL-DR4	Separation (°)
	2016-04-30	3606				
	2016-06-17	3606				
J0758–1451	2016-11-04	3606	119.70000	-14.85278	J0758.8–1450	0.016
J0816–0007	2016-11-05	3616	124.11667	-0.12417	J0816.4–0007	0.006
J0826–5054	2016-11-04	3606	126.53333	-50.91028	J0826.1–5053	0.012
	2017-02-20	3606				
J0838–2827	2016-11-05	3606	129.69583	-28.45667	J0838.7–2827	0.005
	2017-02-16	3606				
	2017-02-16	3606				
	2017-02-16	3606				
	2017-02-16	3606				
	2017-02-17	3606				
	2017-02-17	3606				
	2017-02-20	3606				
	2017-02-21	3606				
	2017-02-22	3606				
J0919–6204	2015-10-17	3606	139.93333	-62.07778	J0919.5–6203	0.027
	2015-10-17	3606				
	2015-10-17	2993				
	2015-11-22	3606				
J0922–6316	2016-02-03	3606	140.55833	-63.26861	J0921.7–6317	0.055
	2016-03-28	3606				
	2016-04-30	1083				
	2016-06-18	3606				
	2017-02-17	3606				
J0933–6233	2016-02-03	3606	143.49167	-62.55028	J0933.8–6232	0.008
	2016-03-28	3606				
	2016-06-18	3606				
J0952–0608	2016-11-04	3606	148.05417	-6.13333	J0952.1–0607	0.008
J0953–1509	2016-11-05	3606	148.40417	-15.15639	J0953.6–1509	0.002
J1107–7724	2016-11-04	3606	166.83750	-77.41639		
J1117–4840	2016-02-03	3606	169.27500	-48.67694	J1117.5–4839	0.076
J1120–2204	2016-11-04	3606	170.00000	-22.07444	J1120.0–2204	0.004
J1126–5006	2017-02-16	3606	171.51250	-50.10833	J1126.0–5007	0.011
	2017-02-21	3606				
J1145–6822	2016-11-04	3606	176.42917	-68.37750	J1146.0–6822	0.033
J1204–5033	2015-10-17	3606	181.16667	-50.55806	J1204.5–5032	0.017
	2015-10-17	3606				
	2015-11-22	3606				
	2015-11-22	3606				
	2015-11-22	1747				
J1207–4536	2017-02-20	3606	181.88333	-45.60028	J1207.4–4536	0.014
J1207–4537	2016-02-03	3606	181.87083	-45.61833	J1207.4–4536	0.006
J1208–5512	2016-11-04	3606	182.12917	-55.20694	J1208.5–5512	0.009
J1236+1129	2017-02-17	3606	189.19583	11.48417	J1235.9+1136	0.240
J1259–8149	2016-11-04	3606	194.85833	-81.82611	J1259.0–8148	0.017
	2017-02-20	2773				
J1304+1203	2016-11-05	3606	196.12083	12.05833	J1304.4+1203	0.006
J1335–5656	2016-02-03	3606	203.77500	-56.93611	J1335.0–5656	0.012
	2017-02-21	3606				
J1345–2612	2016-11-05	3606	206.49167	-26.20778	J1345.9–2612	0.010
J1404–5236	2016-11-05	3606	211.22917	-52.60278	J1404.8–5237	0.028

Table 3 *continued*

Table 3 (continued)

Target	Date	Length (s)	R.A.	Decl.	4FGL-DR4	Separation ($^{\circ}$)
J1416–5021	2017-02-16	3606	214.19583	-50.35833	J1416.7–5023	0.033
	2017-02-22	3606				
J1435–3906	2016-02-03	3606	218.98750	-39.10750		
J1439–5142	2016-02-03	3606	219.78750	-51.70556	J1439.2–5142	0.012
J1512–7132	2015-10-17	698	228.24583	-71.53417	J1513.2–7131	0.026
	2015-10-17	2128				
J1517–4446	2016-11-05	1233	229.37500	-44.76889	J1517.7–4446	0.038
J1526–3811	2016-02-03	3606	231.64167	-38.18417	J1526.6–3810	0.021
J1533–5232	2017-02-16	3606	233.47917	-52.54944	J1534.0–5232	0.013
	2017-02-22	3606				
	2017-03-19	3606				
J1544–2554	2016-11-05	3606	236.05833	-25.91167	J1544.2–2554	0.005
J1555–2908	2017-02-17	3606	238.92083	-44.09250		
J1611–6011	2015-10-18	3606	242.80833	-60.19833	J1611.6–6013	0.059
J1623–6935	2016-02-03	3606	245.95833	-69.58583	J1623.9–6936	0.023
J1639–5146	2017-02-16	3606	249.85000	-51.77611	J1639.3–5146	0.007
	2017-02-22	3606				
	2017-03-19	3606				
J1643–3148	2015-10-18	3606	250.85000	-31.81472	J1643.3–3148	0.008
	2016-02-04	3606				
J1646–4405	2017-02-16	3606	251.59583	-44.09250	J1646.5–4406	0.024
	2017-02-22	987				
	2017-03-19	3606				
J1649–3010	2016-11-05	3606	252.45417	-30.18194	J1649.8–3010	0.003
J1653–0158	2016-11-05	3606	253.40000	-1.97806	J1653.6–0158	0.004
J1656–2733	2016-11-05	2407	254.15000	-27.55694	J1656.5–2733	0.007
J1704–4856	2016-02-03	3606	256.02500	-48.94583	J1705.4–4850	0.251
	2016-03-28	3606				
J1711–3004	2015-10-17	2983	257.78750	-30.06778	J1711.0–3002	0.024
J1715–3324	2016-11-05	3606	258.75000	-33.41222	J1714.9–3324	0.010
	2017-02-22	3606				
	2017-03-19	3606				
J1717–5804	2017-02-16	3606	259.39167	-58.07417	J1717.5–5804	0.008
J1721–5255	2016-11-06	3606	260.29583	-52.92306	J1721.3–5257	0.043
J1739–2530	2017-02-17	3606	264.87917	-25.50472	J1739.3–2531	0.044
J1743–4322	2016-11-06	3606	265.96667	-43.38167	J1743.7–4321	0.032
J1747–3505	2017-02-16	3606	266.75000	-35.09833	J1747.0–3505	0.017
J1759–3849	2016-11-06	3606	269.80833	-38.82278	J1759.1–3849	0.012
	2017-02-13	3606				
J1802–4718	2016-02-03	3606	270.71250	-47.30806	J1802.8–4719	0.011
	2016-03-28	1806				
J1805–3619	2015-10-17	2407	271.25833	-36.33056	J1805.1–3618	0.029
	2015-11-12	646				
J1812–3144	2016-02-03	3606	273.20833	-31.73583	J1812.8–3144	0.012
	2016-03-28	3606				
J1813–6847	2017-02-16	3606	273.39167	-68.78722	J1813.7–6846	0.022
J1816–6405	2016-11-06	3606	274.12083	-64.09861	J1816.4–6405	0.014
	2017-02-13	643				
	2017-02-17	3606				
J1818–3333	2015-11-22	3606	274.50833	-33.56444	J1817.9–3334	0.025
J1822–4717	2016-11-06	3606	275.74167	-47.29750	J1822.9–4718	0.008
	2017-02-17	3606				
J1823–3543	2015-10-18	3606	275.96250	-35.73278	J1823.8–3544	0.009

Table 3 continued

Table 3 (*continued*)

Target	Date	Length (s)	R.A.	Decl.	4FGL-DR4	Separation (°)
J1824–5426	2016-11-06	3606	276.06250	-54.43333	J1824.2–5427	0.019
	2017-02-17	3606				
J1832–3840	2015-10-17	1888	278.23750	-38.67556	J1833.0–3840	0.019
J1844–3840	2017-02-17	3606	281.15000	-38.68056		
J1858–5425	2016-11-06	3606	284.62083	-54.41778	J1858.3–5424	0.027
J1911–4857	2015-10-17	2856	287.86667	-48.95806	J1911.4–4856	0.012
	2015-11-22	3606				
	2016-01-17	3606				
J1956–7012	2016-11-06	3606	299.12500	-70.20833	J1956.6–7011	0.025
J2000–0258	2017-02-17	2603	300.22083	-2.96750		
J2029–4237	2016-11-06	3606	307.37917	-42.63000	J2029.5–4237	0.002
	2017-02-17	3606				
J2045–6835	2016-11-06	3606	311.44583	-68.59917	J2045.9–6835	0.016
	2017-02-17	3606				
J2219–6837	2016-11-06	3606	334.95833	-68.61889	J2219.7–6837	0.004
J2342–4747	2017-02-17	3606	355.69583	-47.78889	J2342.4–4739	0.137
	2017-02-20	3606				
	2017-03-19	3606				
J2355–5247	2016-11-06	3606	358.79583	-52.79389	J2355.2–5247	0.006
	2017-02-13	1303				
	2017-02-17	3606				
J2355–6612	2016-11-06	3606	358.91667	-66.20167	J2355.5–6614	0.034
	2017-02-20	3606				
	2017-03-19	3606				